BNL-107275-2014-CP

Investigation of Heat Pipe Cooling of LI-ION Batteries

Andrey Belyaev

Will be presented at the American Society of Thermal and Fluids Engineers Conference
New York City
August 9 – 12, 2015

December 2014

Nonproliferation and National Security Department

Brookhaven National Laboratory
P.O. Box 5000
Upton, New York 11973
www.bnl.gov

Notice: This manuscript has been authored by employees of Brookhaven Science Associates, LLC under Contract No. DE-AC02-98CH10886 with the U.S. Department of Energy. The publisher by accepting the manuscript for publication acknowledges that the United States Government retains a non-exclusive, paid-up, irrevocable, world-wide license to publish or reproduce the published form of this manuscript, or allow others to do so, for United States Government purposes.

This preprint is intended for publication in a journal or proceedings. Since changes may be made before publication, it may not be cited or reproduced without the author's permission.

DISCLAIMER

This report was prepared as an account of work sponsored by an agency of the United States Government. Neither the United States Government nor any agency thereof, nor any of their employees, nor any of their contractors, subcontractors, or their employees, makes any warranty, express or implied, or assumes any legal liability or responsibility for the accuracy, completeness, or any third party's use or the results of such use of any information, apparatus, product, or process disclosed, or represents that its use would not infringe privately owned rights. Reference herein to any specific commercial product, process, or service by trade name, trademark, manufacturer, or otherwise, does not necessarily constitute or imply its endorsement, recommendation, or favoring by the United States Government or any agency thereof or its contractors or subcontractors. The views and opinions of authors expressed herein do not necessarily state or reflect those of the United States Government or any agency thereof.

BNL-107275-2014-CP

INVESTIGATION OF HEAT PIPE COOLING OF LI-ION BATTERIES

Andrey Belyaev, Dmitriy Fedorchenko, ManapKhazhmuradov, Alexey Lukhanin, OleksandrLukhanin, YegorRudychev
Kharkov institute of physics and technology, Ukraine
Bahram Khalighi, Taeyoung Han, Erik Yen
Vehicle Systems Research Laboratory GM R&D Center
General Motors Global R & D
Upendra S. Rohatgi
Brookhaven National Laboratory, USA

NOMENCLATURE

Q	heat power, W
ITD	inlet temperature difference, K
A	area, m^2
t	temperature, °C
K	thermal conductivity, W/(m·K)
l	length, m
ρ	density, kg/m^3
σ	surface tension, N/m
G	free fall acceleration, m/s^2
Ku	Kutateladze number for heat transfer limit
d	diameter, m
j	heat flux, W/m^2
j^+, j^-	heat fluxes from liquid surface into vapor and in the counter direction, W/m^2
m_0	mass of the molecule, kg
λ	latent heat of vaporization, J/kg
n	concentration of the vapor molecules, m^{-3}
$<v>$	average velocity of the vapor molecule, m/s
k	Boltzmann constant, $k=1.38\cdot10^{-23}$ J/K
T	absolute temperature, K
M	molar mass, kg/mole
R	specific gas constant, R=8.31 J/(mole K)
P	pressure, Pa
q	heat conduction, W/K
Subscripts	
in	Inlet
max	maximum value
min	minimum value
avg	average surface value
e	evaporation
a	adiabatic
surf	surface
l	liquid
v	vapor
s	saturation
rad	radiator

ABSTRACT

Li-Ion batteries are currently used in hybrid and electric vehicles. Battery life and performance requires temperature control in narrow range. One of the methods considered is use of specially designed heat pipe. The study includes a heat pipe between two battery simulators. The heat pipe was cooled by air flow of 2.5 m/s and with temperature range of from 9°C to 40°C.

We have compared the measured surface temperature distributions to those which were received from computer simulation in order to obtain effective thermal conductivity of the heat pipe and its thermal performance. This effective thermal conductivity increases, as the inlet air temperature increases and reaches the value of 2500 W/(m×K).

INTRODUCTION

Nowadays, Li-Ion batteries are widely used as power sources for various devices. But these batteris have tight restrictions on the working temperature, especially for charging mode. The most efficient charging regime of Li-Ion batteries occurs in rather narrow temperature range of 30 – 35 °C and volume temperature differences of several degrees of Celsium [1]. For the temperatures above 40°C, the battery life decreases, while below 10°C, the battery performance degrades and working efficiency substantially decreases.

The heat generation in the Li-ion battery cell depends on the charge/discharge current, which increases with battery use time. We chose the value of the maximum heat generation of 15 watts per each Li-ion battery cell, based on the available calculations and the experimental results [2, 3].

The efficiency of Li-Ion battery cooling process using the heat pipe has been investigated. Cooling efficiency for such system depends on the thermal conditivity of the heat pipe, inlet air temperature and flow rate. The operational performance of cooling system for the temperature range from 9 to 40°C and working regime of heat pipe for these temperatures have been studied.

EXPERIMENTAL SETUP

The experimental setup for studies of cooling system performance includes measurement chamber, power source for battery imitators, air station, airflow rate and temperature measurement system and surface temperature measurement system. The entire setup is schematically shown on the Fig. 1.

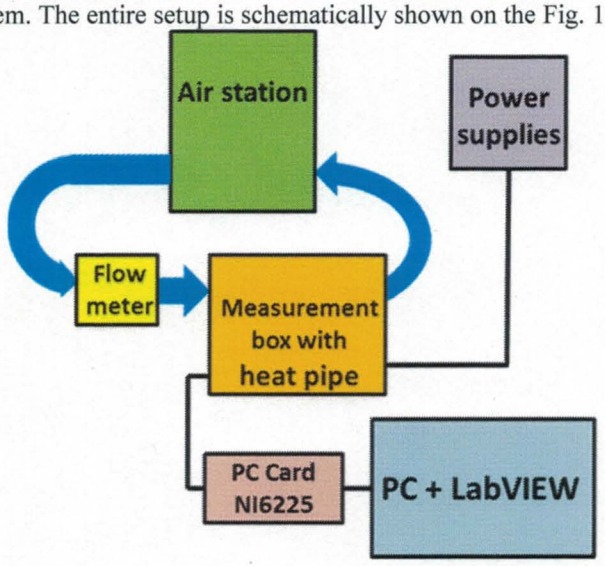

Fig. 1. *Block diagram of the experimental setup for the measurement chamber with heat pipe.*

Instead of the Li-Ion batteries we have used two battery power cells imitators with thermal properties equivalent to the real ones, which were developed earlier [4]. The overall dimension of the cells were 200×150×12 mm. The cells had transversal heat conductivity of 1 W/m K, and longitudinal heat conductivity of 60 W/m K.

To study the cooling process, a measurement chamber for two power cells and a heat pipe was constructed. The gap between the cells was 3 mm. The heat power of each power cell imitator was 7.5 W.

The flat heat pipe size is 220×200×3 mm. It was placed between the power cells. To improve the thermal contact between power cell and heat pipe, we used the heat-conducting paste with thermal conductivity of 1 W/ (m×K). The "hot end" of the heat pipe with the radiator was placed in the airflow channel. The radiator had 11 rectangular copper ribs with 5 mm pitch. Each rib was 0.5 mm thick and had length of 200 mm and width of 27 mm.

The air station provides the inlet airflow rates up to 80 m^3/h, with the temperatures ranging from -20°C to +50°C. The measuring system was based on the NI6225 PC-card and LabView software. It monitored the surface temperature of the imitators. The surface temperature distribution was obtained using temperature sensors TMP36. Each simulator surface holds 20 of such sensors.

The heat pipe, imitators and air channel were thermally insulated from the environment. The air flow, with stabilized temperature, passes through the radiator ribs in the upper part of the heat pipe and removes heat. For the airflow velocity of 2.5 m/s, the pressure drop in the air channel DP (air) was28 Pa for all inlet air temperatures. The design of the measurement chamber is shown on the figure 2.

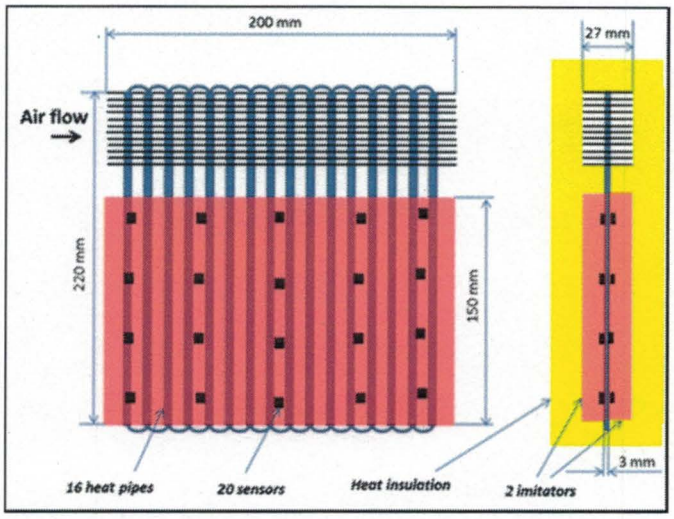

Fig. 2. *Measurement chamber with heat pipe.*

The heat pipe is based on thermo-siphon principle. It consists of 16 thin heat pipes, which are joined in one condensation/evaporation module. Each pipe is made of stainless steel and has diameter of 4 mm with 0.3 mm wall thickness. As the gap between the simulators is 3mm we have to pre-press these cylindrical pipes so they fit inside the channel, and due to the elliptical pipe deformation width becomes 5 mm.

The pipe has inner layer made from stainless steel mesh with mesh size of 0.12mm×0.14mm. This layer provides separation of the vapor flow in the center and liquid flow, and ensures perfect wetting of the side wall. Figure 3 shows the actual heat pipe design.

The cooling liquid (liquid butane) was placed in the tube. In the working mode heat from the cell imitators evaporates the liquid in the lower end of the tube and vapor flows to the upper part where the radiator is placed. Here the vapor condensates and gravity force moves condensate down to the evaporation zone. The mesh-coated walls cause the condensate to move essentially in this mesh layer without undesirable interaction with the counter vapor flow.

Fig. 3. *The design of the heat pipe.*

EXPERIMENTAL RESULTS

Using our experimental setup we have studied the cooling process for inlet air temperature range from 9°C to 40°C. In all cases the air velocity was 2.5 m/s. The heat pipe used butane as working liquid. The main subject of our interest was surface temperature distribution for the power cell imitators. This distribution provides information about average battery temperature regimes and temperature gradients. The measured surface temperature distributions for inlet air temperatures 20°C and 30°C are shown on the Figure 4. Table 1 contains minimum, maximum and average surface temperatures for the different inlet air temperatures.

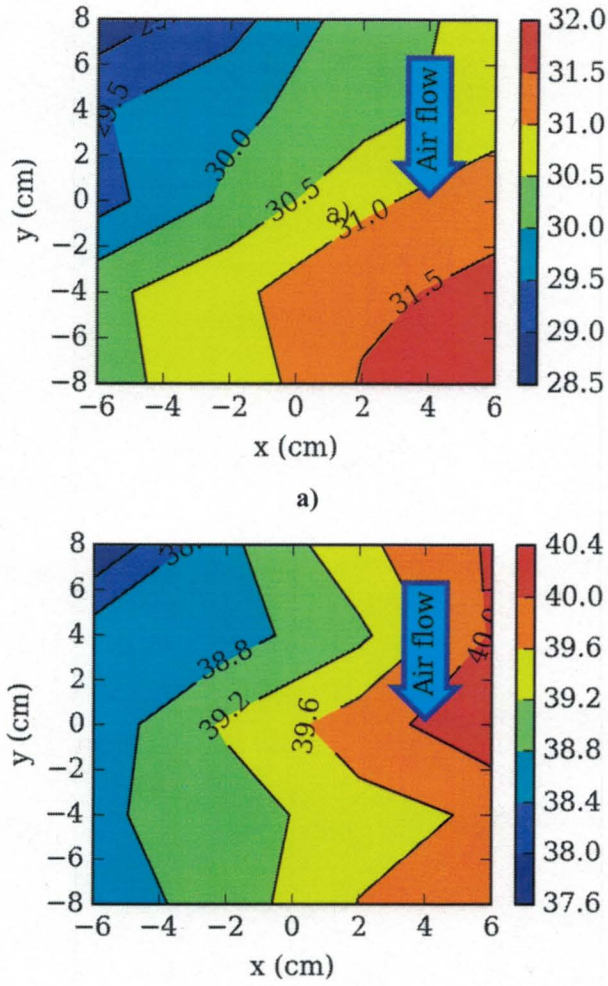

Fig. 4. *The temperature distribution of one simulator surface, at 2.5 m/s air flow rate. Inlet air temperature: a) 20 °C, b) 30.2 °C.*

Table 1. The measurement minimum, maximum and average temperatures for two surfaces of the imitators.

t_{in}, °C	t_{max}, °C		t_{min}, °C		t_{avg}, °C	
Surface	*1*	*2*	*1*	*2*	*1*	*2*
9.0	19.2	19.2	21.1	21.1	20.3	20.3
20.0	28.7	28.4	31.7	31.7	30.5	30.5
30.2	37.8	37.6	40.1	40.3	39.2	39.2
38.6	46.9	46.9	48.2	48.2	47.6	47.6

There are a number of ways to quantitatively estimate cooling efficiency. In our paper we adopt Q/ITD as such parameter. This parameter is defined as

$$Q/\mathrm{ITD} = \frac{Q}{t_{surf} - t_{in}}, \qquad (1)$$

Where Q is heat power, t_{surf} – average surface temperature, t_{in} – inlet air temperature. The denominator in (1) is often called ITD –Inlet Temperature Difference. Using the experimental data from table 1 we obtain cooling efficiency of the heat pipe (see Fig. 5).

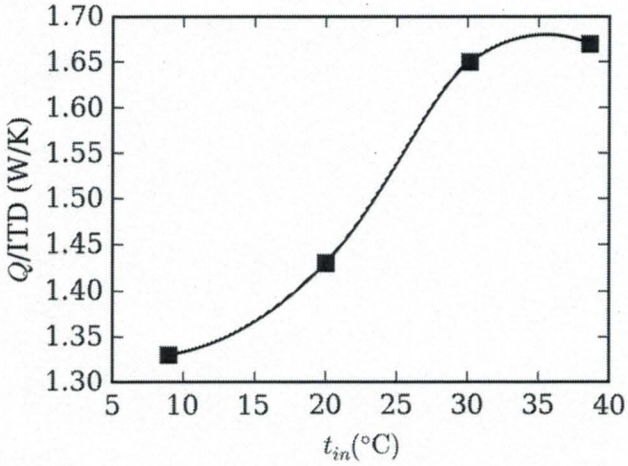

Fig. 5.*The cooling efficiency of the heat pipe.*

The temperature dependence of the cooling efficiency arises from the thermal properties of the liquid-vapor boundary. This effect is discussed in the next section.

NUMERICAL SIMULATION AND ANALYSIS

The numerical simulation of the cooling system includes two stages. During the first stage, we have simulated evaporation and convection in the single tube out of the 16 tubes forming the heat pipe. Our aim was to analyze vapor flow inside the heat pipe, namely, pressure and velocity distribution. On the next stage, we considered the entire cooling system, but we neglected the details of heat transfer inside the heat pipe. This stage helps us to estimate the effective thermal conductivity by comparing results with the experimental results. All simulations were performed using SolidWorks 2011 software with SolidWorks Flow Simulation module [5]. This software is a 3D design framework which works seamlessly with the CFD simulation module. This module uses finite volumes method to address various hydrodynamic and heat transfer problems.

The model for single tube was rectangular parallelepiped with full length of 170 mm and 2mm×4mm cross section. It consisted of evaporation area (l_e=150 mm) and adiabatic area (l_a=20 mm). Our software does not directly support simulation of evaporation process. To overcome this restriction, we considered the evaporation on the inner surface of the heat pipe in the evaporation area as inlet mass flow and manually set the corresponding boundary conditions. Thus instead of two-phase problem with phase transition we obtained the pure hydrodynamic problem for vapor flow inside the heat pipe with inlet mass flow through the side walls.

The corresponding mass flow rate is defined by the heat power applied to the pipe and by evaporation heat of the working liquid. In our case we have heat power of 0.93 W, and for butane we obtain the required mass flow rate of $0.24 \cdot 10^{-5}$ kg/s. As we have to consider the evaporation process at the working temperature 20°C, we specified the butane pressure of 200 kPa.

During the simulation we used meshes containing 48384, 176640 and 573120 cells to decrease the uncertainties due to discretization. The control parameter was average vapor velocity on the outlet. According to the procedure described in [6] the grid convergence index (GCI) was 3.65%. Our software is capable to automatically switch between turbulent and laminar flow mode so we set the corresponding simulation setting to enable this automatic mode selection. As it follows from the simulation results the flow velocity is low and CFD software used the laminar mode during calculations.

Figure 6 contains pressure and vapor velocity distributions in the heat pipe. One can see that flow velocity is rather low and so the corresponding pressure drop due to hydrodynamic drag is low and does not have a substantial effect on the heat transfer.

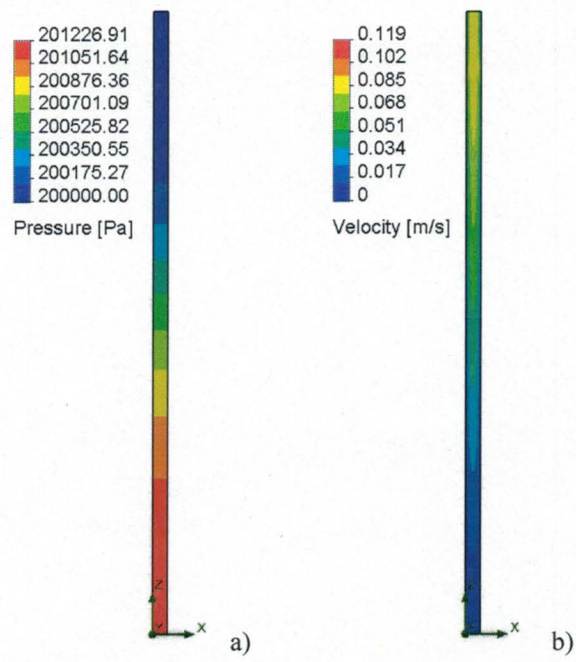

Fig. 6.*Pressure distribution (a) and velocity (b) of butane vapors in the heat pipe at 20 °C*

Considering the working characteristics of the heat pipe using thermo-siphon principle, the entrainment limit [7] must also be estimated. This limit is caused by the interaction of the vapor flow with the counter condensate flow. Vapor flow entrains the condensate in the wall mesh and hinders its transport to the evaporation area. This eventually results in

the condenser flooding and imposes the limit on the heat pipe performance. The corresponding relation for heat transfer limit is given by

$$Q_{\max} = \mathrm{Ku}\,(\rho_v)^{0.5}\left[g(\rho_l - \rho_v)\sigma_l\right]^{0.25}, \qquad (2)$$

Where ρ_l, ρ_v are vapor and liquid densities correspondingly, σ_l is surface tension, g is gravitational acceleration, Ku is Kutateladze number. Kutateladze number is calculated using the following equation [5]

$$\mathrm{Ku} = 0.16\left\{1 - \exp\left[-(d_e / l_e)(\rho_l / \rho_v)^{0.13}\right]\right\}, \qquad (3)$$

Where d_e and l_e are vapor channel diameter and length. For current heat pipe, formula gives the heat transfer limit of 1.189 W while the required heat power is 0.93 W.

During the second stage, we have developed the 3D model of the cooling system (Fig. 7). The geometry and materials of the radiator and power cells are the same as for the real system. The heat pipes are simulated as 16 rectangular cross section pipes with fixed thermal conductivity. We considered a conjugate problem that included conductive heat transfer from the imitator as a power source through the heat pipe and radiator alongside with convective heat transfer from radiator to the cooling air flow.

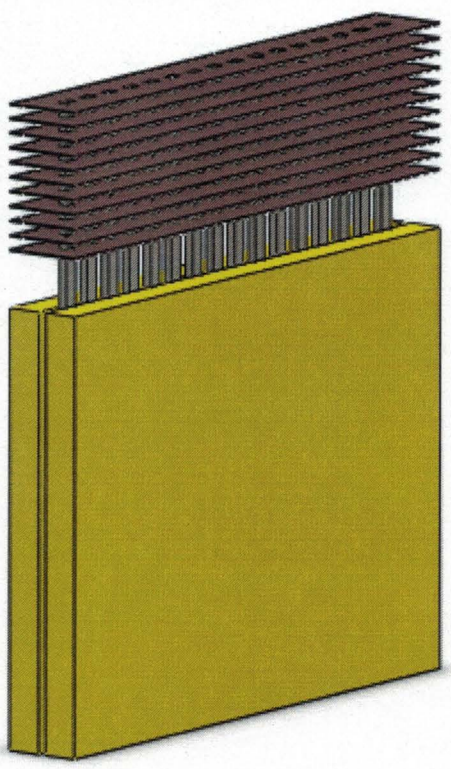

Fig. 7. *CAD model for the cooling heat pipe*

During the calculations the thermal conductivity of the heat pipes was varied in order to fit the calculated average surface temperature of the imitator to the experimental one (see Table 1). This fitting process was repeated for different inlet air temperatures. Table 2 contains the calculated values for imitator surface temperatures and the corresponding thermal conductivities.

Table 2. Simulator surface temperatures and heat pipe thermal conductivity (numerical simulation).

t_{in}, °C	t_{max}, °C	t_{min}, °C	t_{avg}, °C	K, W/(m·K)
9.0	17.1	21.8	20.3	1100
20.0	27.6	31.9	30.4	1450
30.2	37.0	40.5	39.2	2400
38.6	45.4	48.8	47.6	2600

Fitting of the calculated average surface temperature of the imitator to the experimental one ensures the equal Q/IDT values both for numerical simulation and experiment for the corresponding inlet air temperatures. This follows directly from the Q/ITD definition as in Eq. (1). Cooling efficiency for the power cell imitators depends essentially on the heat transfer through the heat pipe and air radiator. Namely, we could write the following relation for our cooling system

$$(Q/\mathrm{ITD})^{-1} = (Q/\mathrm{ITD}_{rad})^{-1} + q^{-1}, \qquad (4)$$

Where Q/ITD_{rad} is defined similar to Eq. (1) as

$$Q/\mathrm{ITD}_{rad} = \frac{Q}{t_{rad} - t_{in}}, \qquad (5)$$

And t_{rad} is average radiator surface temperature. The radiator surface temperatures obtained from the numerical simulation are given in Table 3.

Table 3. Radiator temperatures (numerical simulation).

t_{in}, °C	t_{max}, °C	t_{min}, °C	t_{avg}, °C
9.0	13.4	17.1	15.4
20.0	24.6	28.0	26.6
30.2	34.8	37.8	36.6
38.6	43.4	46.3	45.1

The second term in Eq. (4) describes the heat transfer through the heat pipe. Here q is and average heat conduction of the heat pipe defined as

$$q = \frac{Q}{\Delta T}, \qquad (6)$$

Where ΔT is the difference of average surface temperatures of imitator and radiator. The value of q was calculated from Equation (4) for known Q/ITD and Q/ITD_{rad} values. Figure 8 shows the temperature dependence of all the values from Equation (4).

Results of the calculations show that the cooling efficiency for the radiator is almost constant, while thermal conduction of heat pipe increases with the working temperature increase. This temperature dependence of the thermal conduction of the thermo-siphon based heat pipe is

caused primarily by the properties of the vapor-liquid interface in the evaporation and condensation zones. For the evaporation, the vapor pressure and temperature above the surface must be less than equilibrium value, and for condensation, the vapor pressure and temperature must be higher than the equilibrium values. These temperature drops result in the thermal resistance of the vapor channel of the thermo-siphon process.

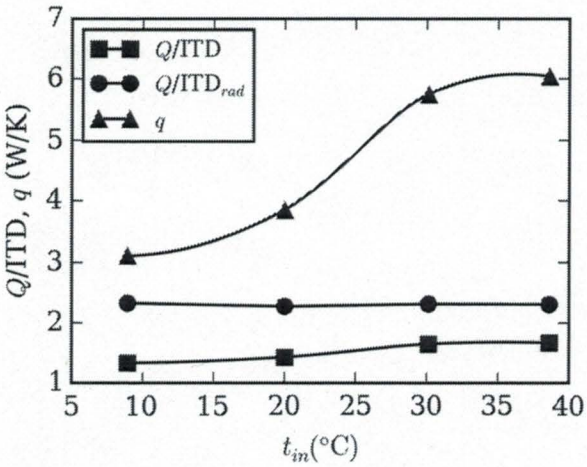

Fig.8. *Dependence of cooling efficiency and thermal conduction coming from inlet air temperature for some chosen heat pipe areas.*

To estimate of the thermal conduction of the vapor-liquid interfaces we can use the simplified kinetic theory of the evaporation and condensation from ref [7]. This approach, however, is valid for the processes not far from the equilibrium state.

According to the above approach the heat flow Q passing through the vapor-liquid interface is given by the balance equation

$$Q / A = j^{+} - j^{-}, \qquad (7)$$

Where A is surface area, j^{+} and j^{-} are heat fluxes from liquid surface into vapor and in the counter direction, respectively. With vapor as perfect gas, the heat flux is defined as,

$$j = \frac{m_0 \lambda n < v >}{4}, \qquad (8)$$

Where m_0 molecular mass, λ is latent heat of vaporization, n is concentration and $< v >$ is average velocity of the vapor molecule

$$< v > = \sqrt{\frac{8kT}{\pi m_0}}, \qquad (9)$$

Where k is Boltzmann constant and T is the gas temperature.

For the perfect gas we have

$$n = \frac{P}{kT}, \qquad (10)$$

Where P is a gas pressure. Using Eq. (10) we can finally get an expression of heat flux as in Eq. (6) in the following form

$$j = \lambda \sqrt{\frac{M}{2\pi RT}} P, \qquad (11)$$

Where M is gas molar mass and R is specific gas constant.

It can be assumed that the vapor layer in the close vicinity of the liquid surface has the same temperature T_l and pressure P_l as evaporating liquid. Thus we can write

$$j^{+} = \lambda \sqrt{\frac{M}{2\pi RT_l}} P_l. \qquad (12)$$

For vapor far from the liquid surface we have

$$j^{-} = \lambda \sqrt{\frac{M}{2\pi RT_v}} P_v, \qquad (13)$$

Where T_v and P are vapor temperature and pressure.

For our working temperatures with sufficient accuracy we can replace both T_l and T_v in Equations (12), and (13) by saturation temperature T_s. Substituting Equations (12) and (13) in Eq. (7) we obtain

$$Q = \lambda A \sqrt{\frac{M}{2\pi RT}} \Delta P, \qquad (14)$$

Where $\Delta P = P_l - P_v$ is pressure drop in the vapor liquid interface.

Using the Clausius–Clapeyron relation for the perfect gas

$$\frac{dP}{dT} = \frac{\lambda M}{RT_s^2} P, \qquad (15)$$

We can rewrite Eq. (14) as

$$Q = \frac{\lambda^2}{\sqrt{2\pi}} \left(\frac{M}{R} \right)^{\frac{3}{2}} A \frac{P}{T_s^{\frac{5}{2}}} \Delta T. \qquad (16)$$

Finally, for the thermal conduction of the vapor-liquid interface we have

$$q = \frac{Q}{\Delta T} = \frac{\lambda^2}{\sqrt{2\pi}} \left(\frac{M}{R} \right)^{\frac{3}{2}} A \frac{P}{T_s^{\frac{5}{2}}}. \qquad (17)$$

The Equation (17) describes the temperature dependence of the heat conduction for the thermo-siphon heat pipe. From the figure 8 it follows that this dependence also defines the temperature dependence of cooling efficiency of the entire system.

We did not expect the quantitative agreement between the Equation (17) and temperature dependence for q depicted in the figure 8. The Equation 17 provides only the temperature dependence for the liquid-vapor interface and for the complex geometry, one should observe considerable discrepancies. Thus we limited ourselves to qualitative assessment. For this purpose, we used the normalized values for q. The normalization factor was q value from Equation (17) and from Table for the average surface temperature 20.3 °C. Also we assumed that saturation temperature T_s is

the same is the working temperature, which in turn is equal to the average surface temperature T_{avg}. The vapor pressure P in Eq. (17) was obtained from the experimental values from the phase diagram for butane.

The results of the comparison are shown on the Figure 9. It follows that the simple kinetic model provides the good description of the temperature dependence of thermal conduction of the heat pipe.

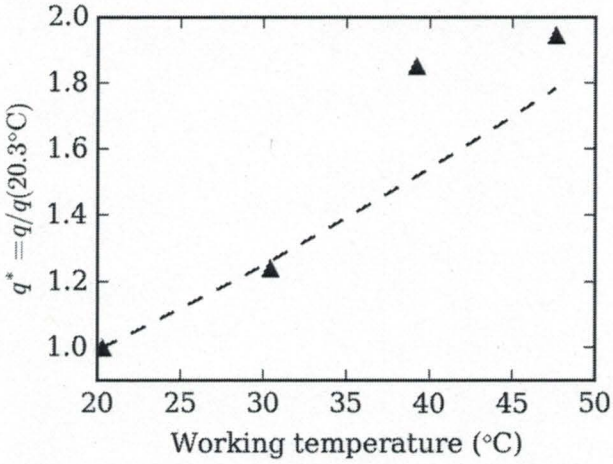

Fig.9.*Comparison of the thermal conduction from Fig. 8 (solid triangles) and from kinetic model (dashed line)*

CONCLUSIONS AND DISCUSSIONS

We have shown that flat multi-sectional heat pipe system provides efficient cooling of the Li-Ion battery. The values of Q/ITD achieved, were between 1.4 – 1.7, for inlet air temperatures of 9°C to 40°C. The battery working temperature was within 20°C – 47°C range and temperature gradient was about 3°C. The effective thermal conductivity was within 1100-2600 W/(m K) range.

The simulation study indicated that the highest thermal resistance appeared at the radiator ribs area, cooled by the airflow. The further improvement of the cooling efficiency will require more efficient radiators for heat pipe.

ACKNOWLEDGMENTS

This research was performed under Department of Energy program of Global Initiative for Proliferation Prevention grant (BNL-T2-371-UA).

REFERENCES

1. Ahmad Pesaran, Matt Keyser, Gi-Heon Kim, Shriram Santhanagopalan, and Kandler Smith. ***Tools for Designing Thermal Management of Batteries in Electric Drive Vehicles.*** Presented at the Large Lithium Ion Battery Technology & Application Symposia Advanced Automotive Battery Conference; Pasadena, CA. February 4–8, 2013. NREL Report No. PR-5400-57747.
2. Taeyoung Han, Gi-Heon Kim, and Lewis Collins. ***Fast-Charging Battery Development: Multiphysics Simulation Tools Power the Modeling of Thermal Management in Advanced Lithium-Ion Battery Systems for Electric Vehicles.*** ANSYS Advantage. Vol. 6(3), 2012; pp. 10-14; NREL Report No. JA-5400-55941.
3. Ui Seong Kim, Jaeshin Yi, Chee Burm Shin, Taeyoung Han, Seongyong Park, ***Modeling the thermal behavior of a lithium-ion battery during charge.*** Journal of Power Sources 196 (2011) 5115–5121.
4. AndreyBelyaev, Alexander Lukhanin, AlexeyLukhanin, Dmitriy Fedorchenko, ManapKhazhmuradov, IgorRudychev, Upendra S. Rohatgi. ***ThermalCharacteristicsofAirFlowCoolingintheLithiumIonBatteriesExperimentalChamber.*** Proc. ASME 2012 Heat Transfer Summer Conference, Volume 1: Heat Transfer in Energy Systems; Rio Grande, Puerto Rico, USA, July 8–12, 2012, pp.129-133.
5. https://www.solidworks.com
6. ***Procedure for Estimation and Reporting of Uncertainty Due to Discretization in CFD Applications,*** J. Fluids Eng. 130, 078001 (2008).
7. D.A. Reay, P.A. Kew, ***Heat Pipes****(Fifth Edition)*, Butterworth-Heinemann, 2006.